Sponge layer feedbacks in middle-atmosphere models

JOURNAL OF GEOPHYSICAL RESEARCH, VOL. 101, NO. D18, PAGES 23,447–23,464, OCTOBER 27, 1996

Sponge layer feedbacks in middle-atmosphere models

T. G. Shepherd, K. Semeniuk, and J. N. Koshyk

Department of Physics, University of Toronto, Toronto, Ontario, Canada

Abstract. Middle-atmosphere models commonly employ a sponge layer in the upper portion of their domain. It is shown that the relaxational nature of the sponge allows it to couple to the dynamics at lower levels in an artificial manner. In particular, the long-term zonally symmetric response to an imposed extratropical local force or diabatic heating is shown to induce a drag force in the sponge that modifies the response expected from the "downward control" arguments of *Haynes et al.* [1991]. In the case of an imposed local force the sponge acts to divert a fraction of the mean meridional mass flux upward, which for realistic parameter values is approximately equal to $\exp(-\Delta z/H)$, where Δz is the distance between the forcing region and the sponge layer and H is the density scale height. This sponge-induced upper cell causes temperature changes that, just below the sponge layer, are of comparable magnitude to those just below the forcing region. In the case of an imposed local diabatic heating, the sponge induces a meridional circulation extending through the entire depth of the atmosphere. This circulation causes temperature changes that, just below the sponge layer, are of opposite sign and comparable in magnitude to those at the heating region. In both cases, the sponge-induced temperature changes are essentially independent of the height of the imposed force or diabatic heating, provided the latter is located outside the sponge, but decrease exponentially as one moves down from the sponge. Thus the effect of the sponge can be made arbitrarily small at a given altitude by placing the sponge sufficiently high; e.g., its effect on temperatures two scale heights below is roughly at the 10% level, provided the imposed force or diabatic heating is located outside the sponge. When, however, an imposed force is applied within the sponge layer (a highly plausible situation for parameterized mesospheric gravity-wave drag), its effect is almost entirely nullified by the sponge-layer feedback and its expected impact on temperatures below largely fails to materialize. Simulations using a middle-atmosphere general circulation model are described, which demonstrate that this sponge-layer feedback can be a significant effect in parameter regimes of physical interest. Zonally symmetric (two dimensional) middle-atmosphere models commonly employ a Rayleigh drag throughout the model domain. It is shown that the long-term zonally symmetric response to an imposed extratropical local force or diabatic heating, in this case, is noticeably modified from that expected from downward control, even for a very weak drag coefficient.

1. Introduction

Haynes et al. [1991] have considered the zonally symmetric response of the middle atmosphere to an imposed extratropical quasi-steady force F, conceived to be associated with the upward propagation and breaking of Rossby and gravity waves. Assuming that the diabatic heating acts to relax temperatures back to some radiatively determined temperature field and that there is a relaxational frictional boundary layer at the ground, Haynes et al. argued that the long-term mean response in the meridional circulation or temperature is exclusively "downward." (In this paper, "heating" is understood to include both positive and negative values.) In particular, an equal and opposite force is induced in the boundary layer through a slight adjustment of the surface winds, which leads to a steady mean meridional circulation extending between the surface and the level of the imposed force. In the vertical branches of this circulation, temperatures are pulled away from radiative equilibrium by adiabatic heating.

It is also instructive to consider the zonally symmetric response to an imposed extratropical quasi-steady diabatic heating Q, conceived to be associated with a change in the radiatively determined temperature due to changes in concentration of radiatively active con-

Paper number 96JD01994.
0148-0227/96/96JD-01994$09.00

stituents. Although *Haynes et al.* [1991] did not explicitly consider this problem, their arguments would imply that the long-term mean response in this case is exclusively local, with a modification of the temperature in the vicinity of the imposed heating and no mean meridional circulation. (This thought experiment was discussed by *McIntyre* [1992, section 6]; see also *Holton et al.* [1995, section 3].)

Of course, any realistic middle-atmosphere model is subject to forcing and diabatic heating throughout its domain. The point of the thought experiments described above is to identify the expected response to a local change in forcing or diabatic heating. Evidently, this response must involve other changes in forcing or diabatic heating in the long-term limit, in order for the model to reach a steady state balance. If these induced changes are complex (involving, for example, $O(1)$ changes in the wave-induced forcing), then the imposed F or Q cannot really be regarded as given and a simple cause-and-effect understanding of the response cannot be obtained. A key assumption of the scenario proposed by *Haynes et al.* [1991] is that such complex feedbacks are second-order effects and the dominant response involves induced changes in two model components that are relaxational and therefore easy to understand, namely, boundary layer frictional drag and radiative heating. Both kinds of induced changes are highly plausible on physical grounds.

Yet many middle-atmosphere models have mechanical drag processes in addition to boundary layer friction that are also relaxational. Two-dimensional models commonly include a Rayleigh drag throughout the model domain, and three-dimensional models commonly include a Rayleigh drag or diffusive sponge layer in the upper portion of the model domain. In both cases the drag acts primarily as a surrogate for missing gravity-wave drag, in order to produce a reasonable climate. Yet its response to perturbations can be expected to be quite different from that of gravity-wave drag, in that a Rayleigh or diffusive drag is relaxational and will thus (like a spring) react with whatever strength is required to oppose an applied force. In contrast, the strength of middle-atmosphere gravity-wave drag is determined by the tropospheric gravity-wave sources; changes in local wind conditions will change where the drag is deposited, but not its total amount. (There could be a small feedback on the tropospheric flow and therefore on the strength of the gravity-wave sources, but for middle-atmosphere drag this should be a second-order effect.) Therefore it is quite possible, as noted by *Haynes et al.* [1991], that middle-atmosphere models with a relaxational drag could respond to an imposed local force or diabatic heating in an unphysical manner.

The purpose of this paper is to explore this possibility. In particular, we consider the long-term zonally symmetric response of a middle-atmosphere model with a Rayleigh-drag sponge layer (in addition to a frictional boundary layer) to an imposed extratropical local force F or diabatic heating Q. (The case of a diffusive sponge layer is briefly considered in section 6 and is found to give a similar response.) The problem is first studied through idealized numerical simulations in section 2. The results suggest a departure from the "downward controlled" response, including significant temperature changes above the level of the imposed force or diabatic heating. In section 3 an asymptotic analysis of the long-term response is performed, extending the results of *Haynes et al.* [1991]; this analysis provides information on parameter dependences. Two experiments with a middle-atmosphere general circulation model are described in section 4, which demonstrate that sponge-layer feedbacks in middle-atmosphere models can be important, in practice. The case of a uniform Rayleigh drag, relevant to many two-dimensional models, is considered in section 5; a noticeable departure from the downward controlled response is also found in this case, even for a very weak drag coefficient. The results are summarized in section 6, and some conclusions are drawn in section 7.

2. Idealized Numerical Solutions

We wish to consider the problem of the zonally symmetric, balanced response to an imposed (switch on) extratropical local force or diabatic heating, in the presence of a lower frictional boundary layer, an upper sponge layer, and Newtonian cooling toward a reference state. For mathematical tractability it is advantageous to consider the limit of small perturbations, with the reference state at rest. *Haynes et al.* [1991] have shown that such an idealization captures the essential nature of the dynamical response in the extratropical middle atmosphere. (The tropics have a different character; see, e.g., *Dunkerton* [1989].)

We thus consider the zonally averaged primitive equations, linearized about a state of rest, under the assumption that the zonal flow remains in geostrophic and hydrostatic balance [see, e.g., *Andrews et al.*, 1987]:

$$\frac{\partial u}{\partial t} - 2\Omega\mu v = F - r(z)u, \tag{1}$$

$$\frac{\partial T}{\partial t} + Sw = Q - \alpha T, \tag{2}$$

$$2\Omega\mu\frac{\partial u}{\partial z} = -\frac{R}{aH}(1-\mu^2)^{1/2}\frac{\partial T}{\partial \mu}, \tag{3}$$

$$\frac{\partial}{\partial \mu}\left[(1-\mu^2)^{1/2}v\right] + \frac{a}{\rho_0}\frac{\partial}{\partial z}(\rho_0 w) = 0. \tag{4}$$

In the above, u, v, and w are the zonal, meridional, and vertical velocities, respectively; $\rho_0(z)$ and $T_0(z)$ are reference profiles of density and temperature, respectively; T is the departure of the temperature from the reference profile; $S = dT_0/dz + \kappa T_0/H$ is a measure of the static stability, where $\kappa = R/c_p$; R is the gas constant, and c_p is the specific heat at constant pressure; H is

the (constant) density scale height; Ω and a are the rotation rate and radius of the Earth, respectively; z is a log-pressure vertical coordinate; and $\mu = \sin\phi$, where ϕ is latitude. The nondivergence condition (4) allows the introduction of a meridional mass stream function ψ defined by

$$v = -\frac{1}{\rho_0(1-\mu^2)^{1/2}}\frac{\partial\psi}{\partial z}, \qquad w = \frac{1}{\rho_0 a}\frac{\partial\psi}{\partial\mu}. \quad (5)$$

We have included a force term in the zonal momentum equation (1) consisting of an imposed (switch on) force per unit mass F together with a Rayleigh drag with a coefficient $r(z)$ that is zero except in the lower frictional boundary layer and the upper sponge layer. In a similar way we have included a diabatic heating in the temperature equation (2) consisting of an imposed (switch on) heating Q together with Newtonian cooling on a timescale $1/\alpha$; making $Q \neq 0$ in a certain region is thus equivalent to changing the radiative equilibrium temperature there. It is appropriate to identify (v, w) in (1)–(5) with the transformed Eulerian mean circulation $(\bar{v}^*, \bar{w}^*)$ in the zonally averaged equations of motion [*Andrews et al.*, 1987]. In the steady state limit, (v, w) can also be identified with the diabatic circulation. The mass stream function ψ is taken to be zero at $\phi = 0°$, $\phi = 90°$, and at the top and bottom of the model. (As shown by *Haynes and Shepherd* [1989], this lower boundary condition involves an approximation, but its effects are unimportant for middle-atmosphere applications.)

We solve (1)–(5) numerically over the northern hemisphere using finite differences on a height-latitude grid. Parameter values are $T_0 = 240$ K, $\alpha = 1/(5\,\text{days})$, $H = 7$ km, $N^2 = 10^{-4}$ s^{-2}, $\rho_0(0) = 1.225$ kg m^{-3}, and $\Omega = 2\pi$ d^{-1}. The model top is placed at $z = 80$ km, and the imposed force and diabatic heating are Gaussian distributions in z and ϕ centered at 40 km and 45°N, with half widths of $\Delta z = 5$ km and $\Delta\phi = 10°$. Their maximum strengths are, respectively, -10 m s^{-1} d^{-1} and 1 K d^{-1}. The vertical grid spacing is 0.4 km, while the horizontal grid spacing is 0.9°. The planetary boundary layer and sponge layer (when applied) are represented by a Rayleigh drag with $r(z)$ given by

$$r(z) = \begin{cases} \dfrac{1}{2\,\text{days}} & 65\text{ km} \le z \le 80\text{ km} \\ \dfrac{1-\cos[\pi(z-60)/5]}{4\,\text{days}} & 60\text{ km} \le z \le 65\text{ km} \\ 0 & 5\text{ km} \le z \le 60\text{ km} \\ \dfrac{1+\cos(\pi z/5)}{6\,\text{days}} & 0\text{ km} \le z \le 5\text{ km}\,. \end{cases} \quad (6)$$

The numerical solutions are carried forward for 1 year. The model has not yet reached a steady state by then, but the results are indicative of the long-term response.

We first consider the case of a localized switch-on (westward) force $F < 0$, with $Q = 0$ (Figure 1). The initial (transient) response is shown in Figure 1a, the sponge-free response after 1 year is shown in Figure 1b, and the response after 1 year in the presence of the sponge is shown in Figure 1c. We consider the sponge-free, downward controlled response (Figure 1b) to be the true response, and differences between Figures 1b and 1c to be a spurious sponge-layer feedback.

The initial response (Figure 1a) is as predicted by the theory of *Eliassen* [1951]: the force acts locally to decelerate the atmosphere but also drives a poleward mean meridional circulation which returns equatorward, partly above but mainly below the forcing region (Figure 1a, top). This meridional circulation causes adiabatic heating that leads to a quadrupole pattern of temperature tendencies $\partial T/\partial t$ (Figure 1a, middle). The net effect is to spread the zonal wind tendencies $\partial u/\partial t$ (Figure 1a, bottom) out in such a way that the combined wind and temperature tendencies are in thermal wind balance (3). The response is elliptic and therefore nonzero everywhere, but it is most pronounced in the vicinity of the forcing.

As the temperature perturbation grows in time, the αT term in (2) becomes increasingly important. Since αT will have the same sign as $\partial T/\partial t$, as the former grows in magnitude, the latter must correspondingly decrease, with the sum of the two balancing $-Sw$ (the mean meridional circulation being essentially prescribed, on these timescales), until eventually $\partial T/\partial t$ shuts off. This local saturation of the response occurs on a timescale of order $1/\alpha$ and leaves a quasi-steady local balance between adiabatic heating and diabatic heating. (If the forcing region is "tall" then the saturation timescale may be considerably longer; see *Haynes et al.* [1991].) As described by *Haynes et al.* [1991], the meridional cells then "burrow" both upward and downward, away from the forcing region, with the mass flux of the lower cell slowly increasing at the expense of the upper cell. The cells eventually run into the upper and lower boundaries. In the presence of relaxational drag processes near those boundaries, the negative zonal wind acceleration driven by the equatorward meridional circulation induces positive drag forces.

When the drag is purely at the lower boundary, as envisaged by *Haynes et al.* [1991], the upper cell dies away, leaving only the lower cell (Figure 1b, top). The associated temperature change is located exclusively between the ground and the forcing region, in a dipole pattern (Figure 1b, middle), and is maintained by the meridional circulation. Because of the decreasing density with height, a constant mass flux translates into an exponentially decreasing temperature change as one moves down from the forcing level. The positive meridional temperature gradient below the forcing region leads, through (3), to a negative change in the zonal wind both below and above the forcing region, flanked by positive values, with no vertical shear above the forcing (Figure 1b, bottom).

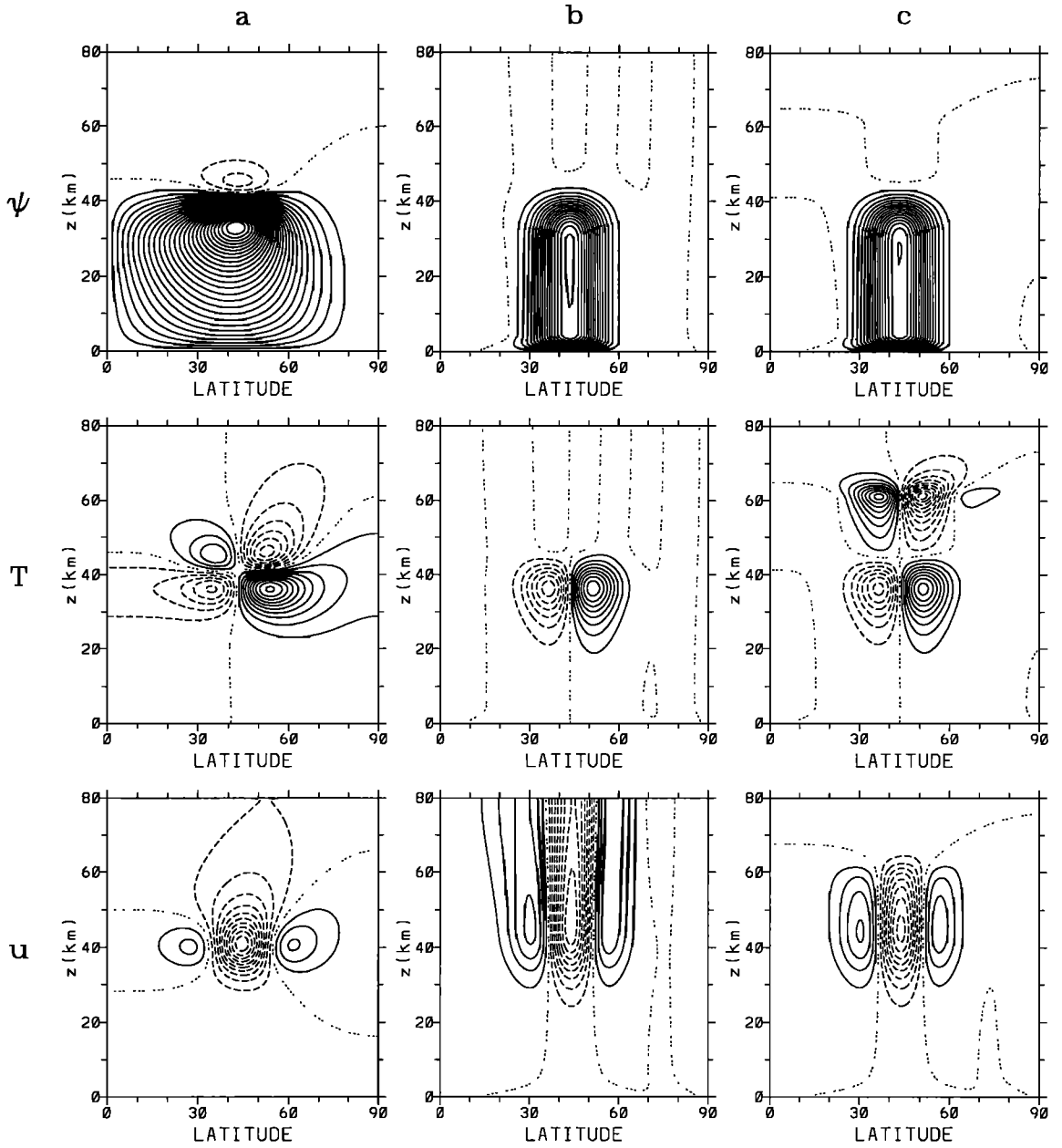

Figure 1. Numerical solutions of (1)–(5) for an imposed negative Gaussian force $F < 0$ centered at 40 km and 45°N, with a maximum strength of -10 m s^{-1} d^{-1}. The model lid is at 80 km, and the sponge begins at 60 km, ramping up to a constant value of $r = 1/(2\,\text{days})$ between 65 and 80 km; density scale height $H = 7$ km; and $\alpha = 1/(5\,\text{days})$. (a) Instantaneous response, (b) model response after 1 year with no sponge layer, and (c) model response after 1 year with the sponge layer. Shown for each response are the meridional mass stream function ψ (top), the temperature perturbation T (middle), and the zonal wind perturbation u (bottom). In Figure 1a, the tendencies $\partial T/\partial t$ (middle) and $\partial u/\partial t$ (bottom) are shown. Contour intervals are as follows: Figure 1a (top), 0.5 kg m^{-1} s^{-1}; Figures 1b and 1c (top), 2.0 kg m^{-1} s^{-1}; Figure 1a (middle), 0.1 K d^{-1}; Figures 1b and 1c (middle), 2.0 K; Figure 1a (bottom), 0.4 m s^{-1} d^{-1}; Figures 1b and 1c (bottom), 20 m s^{-1}.

When, however, the relaxational drag is also exerted through an upper sponge layer, a positive force is induced at the top as well as at the bottom of the model, and the upper cell can persist indefinitely. The long-term response consists of meridional cells both above and below the forcing region, although in this case the force is imposed sufficiently far away from the sponge, about three scale heights away, that the upper cell is practically invisible (Figure 1c, top). Yet its effect is clearly seen in the temperature change, which is now a vertically elongated quadrupole (Figure 1c, middle); the constant mass flux above the forcing level translates into

an exponentially increasing temperature change as one moves up. The zonal wind change is similar to the previous case below the forcing region but decreases with height above the forcing region (Figure 1c, bottom). Another way to understand the response in this case is that the downward controlled response (Figure 1b) implies negative zonal wind accelerations in the sponge layer, which induce positive drag forces. The combined response is thus consistent with downward control, so long as one considers the induced positive sponge-drag force together with the imposed negative force F.

In terms of temperature, the sponge-layer feedback is comparable in magnitude to the presumably real, downward controlled response. The temperature changes below the level of the imposed force are, in this case, essentially unaffected by the sponge (compare Figures 1b and 1c, middle), but if one presumes that all portions of the model atmosphere below the sponge are of physical interest (this is usually the criterion that dictates the position of the sponge) then one must conclude that the sponge induces spurious temperature and zonal wind effects that are quantitatively significant.

We next consider the case of a localized switch-on (positive) diabatic heating $Q > 0$, with $F = 0$ (Figure 2). The initial response (Figure 2a) is again predicted by the theory of *Eliassen* [1951]: the heating acts locally to warm the atmosphere (Figure 2a, middle) but also drives a rising mean meridional circulation which returns downward on either side of the heating region (Figure 2a, top). This meridional circulation causes Coriolis forces that lead to a quadrupole pattern of zonal wind tendencies $\partial u/\partial t$ (Figure 2a, bottom). The net effect is to spread the temperature tendencies $\partial T/\partial t$ (Figure 2a, middle) out in such a way that the combined wind and temperature tendencies are in thermal wind balance.

As described above, the relaxational heating term acts to saturate the temperature response in the vicinity of the imposed diabatic heating on a timescale of order $1/\alpha$, and the two meridional cells then burrow upward and downward away from the region of imposed heating, until they hit the upper and lower boundaries. When the drag is purely at the lower boundary (Figure 2b), then any induced drag force cannot be balanced elsewhere in the atmospheric column (as is required under steady state conditions) and the circulation must eventually collapse. In fact, in this case there is some circulation remaining after one year (Figure 2b, top), but this is a transient effect. The temperature response has already confined itself to the vicinity of the imposed diabatic heating (Figure 2b, middle), producing a dipole barotropic zonal wind change above (Figure 2b, bottom).

In contrast, when the relaxational drag is also exerted through an upper sponge layer (Figure 2c), the Coriolis forces imposed at the top and the bottom are of opposite sign within each column and the induced drag forces can therefore balance each other indefinitely. In this case the two-cell meridional circulation can and does persist (Figure 2c, top); moreover, it is quite broad. It might be thought that the breadth of this circulation is a transient effect, that the circulation would eventually collapse onto the latitude band of the heating region. This is not the case, however, as can be seen from the fact that there is a strong meridional flow in Figure 2c (top) in both the sponge layer and the frictional boundary layer, extending right to the equator. In fact, it is clear that if the transient circulation of Figure 2b (top) is removed from Figure 2c (top), then what is left is a pair of cells extending through the depth of the model atmosphere, with essentially vertical flow in the drag-free regions. These cells persist indefinitely, being driven by the drag force that has spun up in the sponge layer, and there is nothing to force them to be meridionally confined.

Despite the breadth of this sponge-induced meridional circulation, the temperature change associated with it is in this case largely confined to its ascending branch. The combined temperature response (Figure 2c, middle) is a superposition of local warming in the vicinity of the imposed diabatic heating, essentially unchanged from the sponge-free case (Figure 2b, middle), together with a sponge-induced cooling that decreases exponentially as one moves down from the sponge. The maximum value of this sponge-induced cooling is comparable to the maximum value of the warming below.

Therefore the presence of an upper sponge layer is seen to significantly affect the zonally symmetric response to an imposed extratropical local force or diabatic heating. It does this by allowing a drag force to develop in the sponge, which then drives a circulation extending through the entire depth of the model. Although the sponge-layer feedback is attenuated by the density decrease with height, it still has a significant impact on the temperature response just below the sponge, even when the imposed force or diabatic heating is located about three scale heights away from the sponge. The asymptotic analysis in the next section shows that this is always the case, no matter how far away the sponge is from the imposed force or diabatic heating. It should also be noted that the sponge-layer feedback is not latitudinally confined to the region of the imposed force or diabatic heating. This effect, which is another departure from downward control, is particularly evident in the case of the imposed diabatic heating, where the sponge-free circulation vanishes.

The parameter dependences of this sponge-layer feedback will be quantified by means of an asymptotic analysis in the next section. Before doing so, we consider one more idealized numerical solution, motivated by the following considerations. The available evidence [e.g., *Holton*, 1982; *Garcia and Solomon*, 1985; *Shine*, 1989] suggests that most of the middle-atmosphere gravity-wave drag is imposed in the upper mesosphere and mesopause regions. It is generally accepted that this drag is crucial for determining the temperature struc-

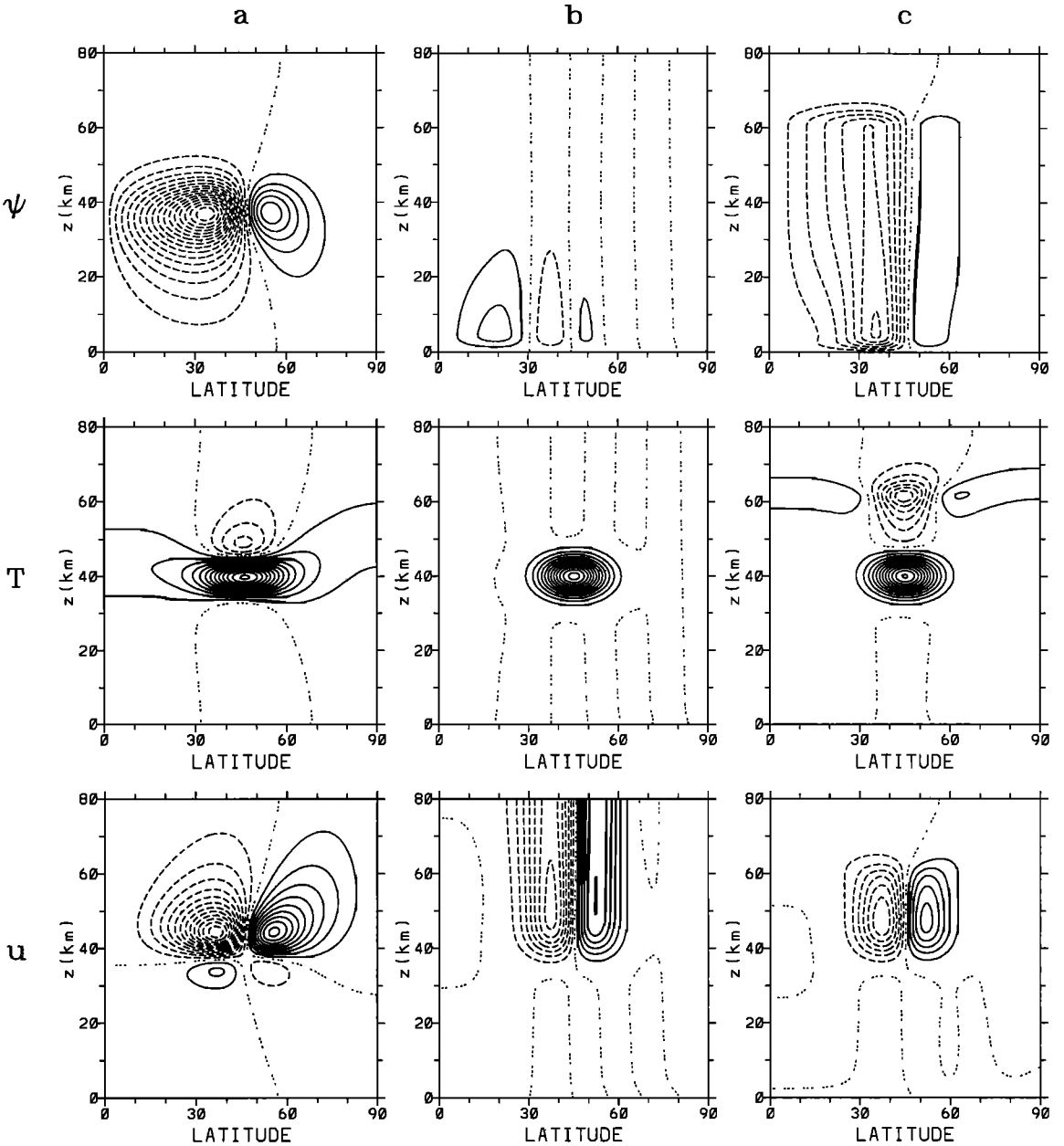

Figure 2. Same as in Figure 1, except for an imposed positive diabatic heating with maximum strength of 1 K d^{-1}. In Figures 2a–2c (top) the meridional cells are ascending at 45°N. Contour intervals are as follows: Figure 2a (top), 0.1 kg m^{-1} s^{-1}; Figures 2b and 2c (top), 0.02 kg m^{-1} s^{-1}; Figure 2a (middle), 0.04 K d^{-1}; Figures 2b and 2c (middle), 0.4 K; Figure 2a (bottom), 0.05 m s^{-1} d^{-1}; Figures 2b and 2c (bottom), 2.0 m s^{-1}.

ture in the mesosphere [e.g., *Andrews et al.*, 1987], possibly down to the middle stratosphere in polar regions [*Haynes et al.*, 1991; *Garcia and Boville*, 1994]. However, in most middle-atmosphere general circulation models the lid is no higher than the mesopause and any sponge layer is therefore acting in the upper mesosphere. This implies that gravity-wave drag parameterization schemes in such models will be applying the bulk of their drag within the sponge layer. It is therefore interesting to consider the extent to which the response to an imposed drag force is modified when the drag is imposed within the sponge layer itself.

This case is shown in Figure 3, which corresponds to Figure 1 but with the imposed force centered at 73 km, in the heart of the sponge layer. As before, the instantaneous response is shown in Figure 3a, the sponge-free long-term response is shown in Figure 3b, and the long-term response in the presence of the sponge is shown in Figure 3c. By comparing Figures 3b and 3c, it is evident that the sponge completely distorts the long-term

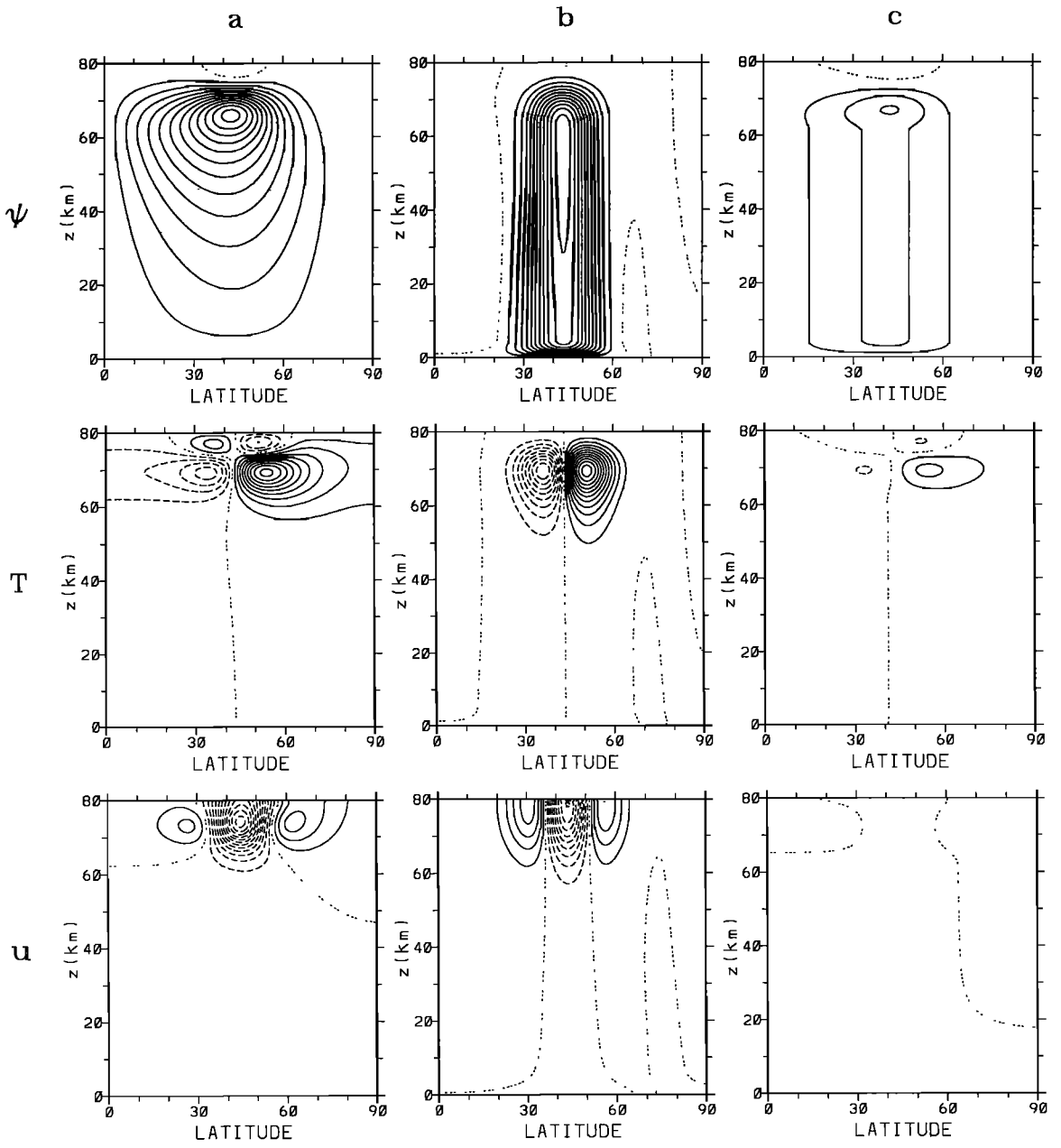

Figure 3. Same as in Figure 1, except for an imposed force located within the sponge layer. Contour intervals are as follows: Figure 3a (top), 0.01 kg m^{-1} s^{-1}; Figures 3b and 3c (top), 0.025 kg m^{-1} s^{-1}; Figure 3a (middle), 0.1 K d^{-1}; Figures 3b and 3c (middle), 1.5 K; Figure 3a (bottom), 0.3 m s^{-1} d^{-1}; Figures 3b and 3c (bottom), 20 m s^{-1}.

response. The mass circulation (Figures 3b and 3c, top) is weakened in overall strength by about a factor of 5 and is spread over the entire hemisphere, instead of being confined directly below the force. The temperature response (Figures 3b and 3c, middle) is likewise weakened, by a factor of 5 to 10 in its maximum values, and is meridionally broadened and vertically shortened. This suggests that the response to the imposed force has been almost completely nullified by the sponge; in addition, a spurious mass circulation has developed that forces (weak) temperature changes over all latitudes.

3. Asymptotic Solutions

In this section we consider asymptotic solutions of (1)–(5) in the long-time limit, following *Haynes et al.* [1991]. For consistency with Haynes et al., we set $z = 0$ at the level of the imposed force or diabatic heating. The upper boundary is then at $z_t > 0$, and the lower boundary is at $z_0 < 0$. The sponge and the planetary boundary layer are represented with a Rayleigh-drag coefficient given by $r(z) = \tilde{r}\mathcal{H}(z - z_s) + \gamma\delta((z - z_0)/H)$, where $\delta(\cdot)$ is the Dirac delta function and $\mathcal{H}(\cdot)$ is the

Heaviside step function and where $0 < z_s < z_t$. The fields are decomposed into a Hough-mode representation (see appendix), in which case (A1)–(A4) may be combined into the single equation

$$\left(\frac{\partial}{\partial t}+\alpha\right)\frac{1}{\rho_0}\frac{\partial}{\partial z}\left(\rho_0\frac{\partial u_n}{\partial z}\right)+\frac{\epsilon_n N^2}{4\Omega^2 a^2}\left(\frac{\partial}{\partial t}+r\right)u_n$$

$$=\frac{\epsilon_n N^2 F_n}{4\Omega^2 a^2}-\frac{\epsilon_n R}{2\Omega a\rho_0 H}\frac{\partial}{\partial z}(\rho_0 Q_n), \qquad (7)$$

where $N^2 \equiv RS/H$ is taken to be constant.

We first consider the case of an imposed force $F_n(z,t) = f_n\mathcal{H}(t)\delta(z/H)$, with $Q_n = 0$. *Haynes et al.* [1991, equation (3.21)] showed that the intermediate-time response consists of upward and downward propagating adjustments. After a time $t \sim b_n z_s/\alpha H$, the upward propagating adjustment encounters the sponge layer and induces a "sponge force" that causes a downward propagating adjustment just like the original one; the resulting sponge-induced modification to the zonal wind u_n^s takes the form

$$u_n^s \sim \eta\frac{f_n b_n}{2\alpha}e^{(z-z_s)/H} \times \operatorname{erfc}\left\{-\left(t+\frac{b_n z'}{\alpha H}\right)\left[\frac{H\alpha^2}{4b_n(b_n+1)|z'|}\right]^{1/2}\right\}, \qquad (8)$$

where $z' \equiv z - 2z_s$, $b_n \equiv -\epsilon_n N^2 H^2/4\Omega^2 a^2$, and

$$\eta \equiv \frac{1-\lambda}{1+\lambda}\left\{\frac{1-\exp[\lambda(z_s-z_t)/H]}{1-\left(\frac{1-\lambda}{1+\lambda}\right)^2\exp[\lambda(z_s-z_t)/H]}\right\}, \qquad (9)$$

with $\lambda \equiv [1+(4b_n\tilde{r}/\alpha)]^{1/2}$. The latitudinal distribution of this sponge force is not the same as that of the imposed force f_n, since η depends on n. When the original downward propagating adjustment encounters the planetary boundary layer, an upward propagating adjustment u_n^b is induced, which is given by *Haynes et al.* [1991, equation (5.4)]. In the presence of both upper and lower boundaries the long-term response then consists of an infinite series of responses from each boundary to the adjustments induced by the other. In the steady state limit we obtain

$$u_n \sim \frac{f_n b_n}{\alpha[1-\eta\xi e^{-(z_s-z_0)/H}]}\begin{cases}1+\eta e^{(z-z_s)/H}+\xi e^{z_0/H}+\eta\xi e^{(z-z_s+z_0)/H}, & 0<z<z_s\\ e^{z/H}+\eta e^{(z-z_s)/H}+\xi e^{z_0/H}+\eta\xi e^{-(z_s-z_0)/H}, & z_0<z<0\end{cases} \qquad (10)$$

where $\xi \equiv (\alpha/b_n\gamma)-1$. The part of u_n in (10) associated directly with the imposed force does not contain η or ξ. Terms that involve η but not ξ represent the sponge response to the u_n induced by the imposed force, without any feedback from the planetary boundary layer. Terms that involve ξ but not η are the response of the planetary boundary layer to this same u_n, without any feedback from the sponge layer. (Note that with $\eta = 0$, (10) reduces as expected to the result given by *Haynes et al.* [1991, equations (3.21) and (5.4)].) The remaining terms represent the infinite series of responses of the sponge to the u_n induced by the planetary boundary layer and vice versa. (A more revealing form of (10), which shows this infinite series of responses, is obtained by expanding the factor $[1-\eta\xi e^{-(z_s-z_0)/H}]^{-1}$ in $\eta\xi e^{-(z_s-z_0)/H}$.)

For reasonable values of the parameters, $\xi e^{z_0/H}$ will be extremely small for a force imposed many scale heights away from the lower boundary; hence the terms involving ξ will be negligible for practical purposes and the steady state response will be given to good approximation by

$$u_n \sim \frac{f_n b_n}{\alpha}\begin{cases}1+\eta e^{(z-z_s)/H}, & 0<z<z_s\\ e^{z/H}+\eta e^{(z-z_s)/H}, & z_0<z<0\end{cases}. \qquad (11)$$

Some of the parameter dependences of η are explored in Figure 4, where it is seen that for reasonable values of the model parameters, $\eta \approx -0.5$. In fact, it is easily seen from (9) that $\eta \sim -1$ in the limit $b_n\tilde{r}/\alpha \gg 1$, this limit being of some relevance to middle-atmosphere models. In short, η can be expected to be an order unity, negative number.

The sponge-layer feedback therefore reduces the zonal wind change nearly to zero just below the sponge, with the effect exponentially decreasing as one moves down. This explains the results seen in Figures 1b and 1c (bottom). The corresponding temperature change can be inferred from (A3); in the steady state limit, neglecting the terms involving ξ,

$$T_n \sim \frac{f_n N^2 H^2}{2\Omega a R\alpha}\begin{cases}\eta e^{(z-z_s)/H}, & 0<z<z_s\\ e^{z/H}+\eta e^{(z-z_s)/H}, & z_0<z<0\end{cases}. \qquad (12)$$

The magnitude of the (spurious) sponge-induced temperature change just below the sponge is seen to be comparable to the (presumably real) temperature change just below the imposed force; both decrease exponentially in z as one moves down. This explains the results seen in Figures 1b and 1c (middle).

To determine the effect on the meridional mass circulation, note that in the steady state limit, (A2) and (A5) imply $\psi_n = -(\rho_0 a\alpha/S)T_n$. The $e^{z/H}$ factors in T_n seen in (12) are therefore removed when it comes to ψ_n, and we find meridional cells of opposite orientation above and below the forcing, with a ratio in strength given by (again ignoring the small corrections involving ξ)

$$\frac{\text{mass flux in upper cell}}{\text{mass flux in lower cell}} \sim \frac{\eta e^{-z_s/H}}{1+\eta e^{-z_s/H}}. \qquad (13)$$

When the sponge is several scale heights away from the forcing level, its effect on the mass circulation is thus seen to be small. This explains the results seen in Figures 1b and 1c (top). Yet even the weak upper cell is seen to have significant effects on the temperature structure within one or two scale heights of the sponge.

Haynes et al. [1991, p. 668a] did, in fact, briefly consider the case where the "surface" drag was imposed above the level of the forcing. In that case they found a reduction in the strength of the lower cell of order $e^{-z_s/H}$ for $b_n\gamma/\alpha \gg 1$, which is consistent with (13).

We now consider the case of an imposed diabatic heating, $Q_n(z,t) = q_n\mathcal{H}(t)\delta(z/H)$, with $F_n = 0$. The analysis proceeds much as above. The sponge-induced fields behave as if they originated from a switch-on forcing at the base of the sponge; for intermediate times, before feedback from the planetary boundary layer, the sponge-induced modification to the zonal wind takes the form

$$u_n^s \sim \eta \frac{q_n b_n \Omega a R}{N^2 H^2 \alpha} e^{(z-z_s)/H} \times \mathrm{erfc}\left\{-\left(t + \frac{b_n z'}{\alpha H}\right)\left[\frac{H\alpha^2}{4b_n(b_n+1)|z'|}\right]^{1/2}\right\}. \quad (14)$$

In the steady state limit we find

$$u_n \sim \frac{q_n b_n 2\Omega a R}{N^2 H^2 \alpha(1-\eta\xi e^{-(z_s-z_0)/H})} \times \begin{cases} 1+\eta e^{(z-z_s)/H}, & 0 < z < z_s \\ \eta e^{(z-z_s)/H} + \eta\xi e^{-(z_s-z_0)/H}, & z_0 < z < 0\,. \end{cases} \quad (15)$$

As above, the terms involving ξ, which reflect the feedback from the planetary boundary layer, are negligible for a diabatic heating imposed many scale heights away from the lower boundary and the long-term response is then given, to good approximation, by

$$u_n \sim \frac{q_n b_n 2\Omega a R}{N^2 H^2 \alpha} \begin{cases} 1+\eta e^{(z-z_s)/H}, & 0 < z < z_s \\ \eta e^{(z-z_s)/H}, & z_0 < z < 0\,. \end{cases} \quad (16)$$

This explains the results seen in Figures 2b and 2c (bottom). The corresponding steady state temperature change is

$$T_n \sim \frac{q_n \eta e^{(z-z_s)/H}}{\alpha} + \frac{q_n}{\alpha}\delta(z/H). \quad (17)$$

As in the case of the imposed force, the sponge-induced temperature change is oppositely signed to the temperature change at the level of the imposed heating and achieves a comparable magnitude just below the sponge (allowing for integration over the δ function, of course). This explains the large sponge-induced cooling above the level of imposed heating seen in Figure 2c (middle). The meridional mass circulation in this case is entirely due to the sponge and may be calculated from $\psi_n = -(\rho_0 a\alpha/S)T_n$; it extends through the depth of the atmosphere with a vertically uniform mass flux (see Figure 2c, top). That the sponge-induced response has a different latitudinal structure than the imposed heating is again explained by the fact that η depends on n.

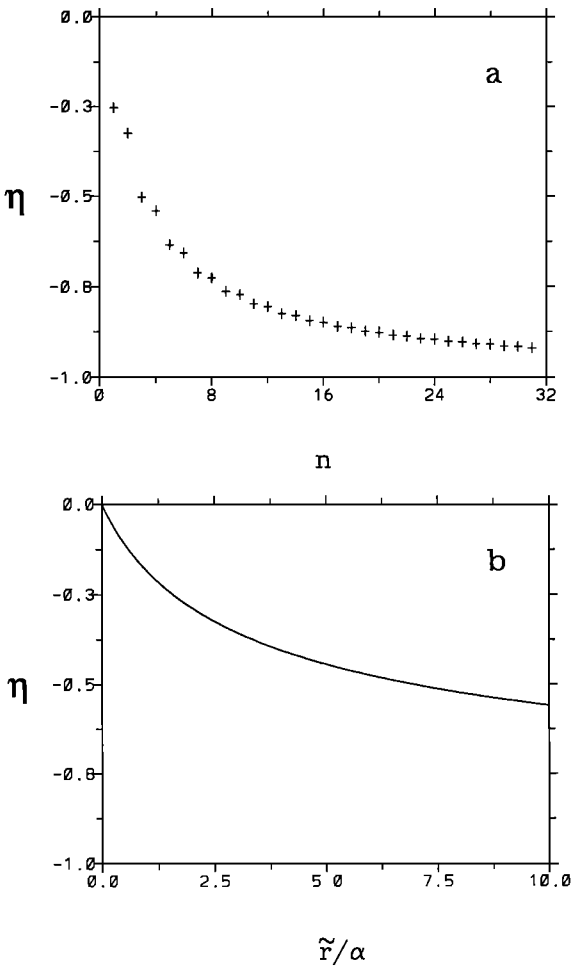

Figure 4. Dependence of η [defined in (9)] on n and $\tilde{r}/\alpha$, with fixed parameters (a) $\tilde{r}/\alpha = 2.5$ and (b) $n = 2$. In both cases, $z_t - z_s = 17.5$ km and $H = 7$ km.

4. Experiments With a Middle-Atmosphere General Circulation Model

In this section, sponge-layer feedbacks are examined in a developmental version of the first-generation Canadian middle-atmosphere model (CMAM). The model is based on a developmental version of the third-generation Canadian Climate Centre (CCC) general circulation model (GCM); the second-generation CCC GCM is described by *McFarlane et al.* [1992]. The CMAM is briefly described by *Shepherd* [1995], and a full description is provided by S.R. Beagley et al. (The radiative-dynamical climatology of the first-generation Canadian Middle Atmosphere Model, submitted to *Atmosphere-Ocean*, 1996). Triangular spectral truncation at wavenumber 32 (T32) and 50 vertical levels between the

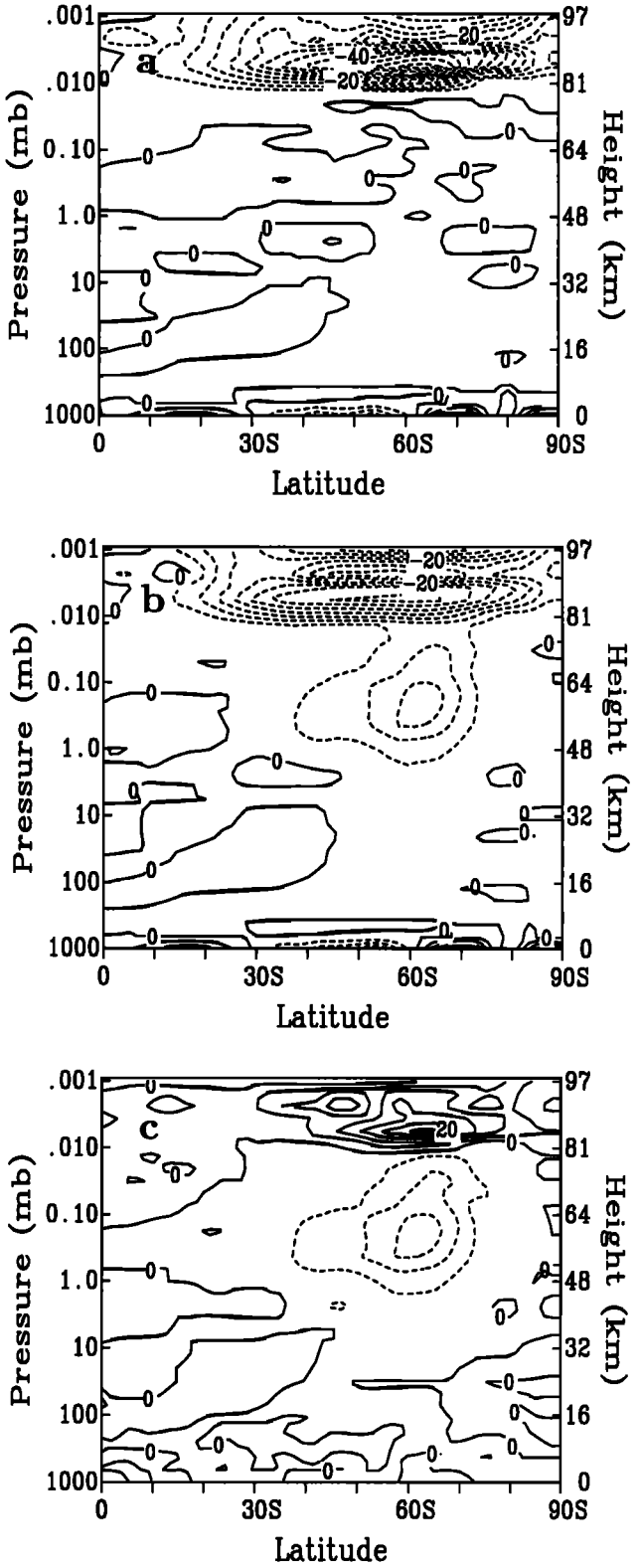

Figure 5. (a) Zonally and temporally averaged sponge-layer plus planetary boundary layer zonal momentum forcing from the Canadian middle-atmosphere model (CMAM) control run for a single June-July-August season. (b) Same as Figure 5a, but for a run including surrogate mesospheric gravity-wave drag centered near (60°S, 0.1 mbar). (c) The difference between the fields in Figures 5a and 5b, i.e., Figure 5b minus Figure 5a. Contour intervals are 5 m s^{-1} d^{-1}.

ground and 0.001 mbar define the model resolution, with an approximate vertical resolution of 3 km above the tropopause. The sponge layer consists of Rayleigh drag with a maximum relaxation coefficient of 1.0 d^{-1}, acting on the horizontal wind above 0.01 mbar.

One major discrepancy between CMAM and observations is that the model overestimates the magnitude of the southern hemisphere wintertime mesospheric zonal jet by almost a factor of 2. This problem is common to many middle-atmosphere models [e.g., *Hamilton et al.*, 1995; *Boville*, 1995] and is at least partly associated with the inadequate representation of mesospheric gravity-wave drag (GWD) effects. Although some mesospheric drag is generated over the Antarctic plateau in CMAM by the orographic GWD parameterization of *McFarlane* [1987], this is insufficient to correct the excessive zonal winds.

Figure 5a shows the temporally and zonally averaged sponge-layer plus planetary boundary layer zonal momentum forcing obtained from the model in the standard configuration for a single June-July-August (JJA) season (the control run). In an attempt to reduce the excessive zonal winds associated with this model (not shown), a second version of CMAM was developed. This version includes an additional forcing that can be considered a crude surrogate for missing mesospheric gravity-wave drag (the wave drag run). The additional forcing consists of Rayleigh drag F, which is activated only when the local horizontal wind speed in the model exceeds 100 m s^{-1} and which has a damping coefficient proportional to the excess.

Figure 5b shows the sponge-layer plus planetary boundary layer forcing for the wave drag run together with the additional Rayleigh drag F, temporally and zonally averaged over the same JJA season. Comparison of Figure 5a to 5b indicates that F has a maximum amplitude of about 15 m s^{-1} d^{-1} at approximately 60°S and 0.1 mbar. The difference between the fields shown in Figures 5a and 5b is displayed in Figure 5c, which demonstrates that the drag on the zonal wind associated with F (negative-valued, dashed contours) is accompanied by a decrease in the magnitude of the sponge-layer forcing (positive-valued, solid contours). Thus, compared with the control run, a positive force is induced within the sponge layer in the wave drag run.

This change in the sponge-layer drag is consistent with the arguments of section 2. From (1) the steady state zonal momentum balance in the model sponge layer can be approximately expressed as

$$-2\Omega\mu v = F_s, \tag{18}$$

where F_s is the forcing provided by the sponge. When F is initially applied in the model, a transient picture not unlike that of Figure 1a (top) emerges, adding an equatorward component to the meridional wind (i.e., $\Delta v > 0$) above the forcing region. As this meridional wind change works its way up into the sponge layer, F_s

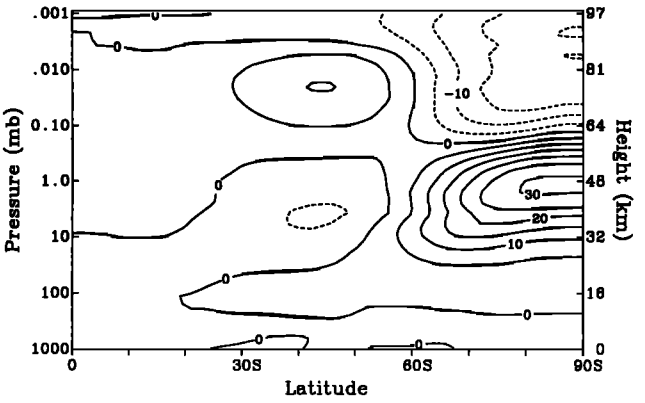

Figure 6. Zonally and temporally averaged temperature difference between the CMAM control run and a run including surrogate mesospheric gravity-wave drag for the June-July-August season. Contour interval is 5 K.

adjusts to smaller negative values. Thus, as shown in Figure 5c, $\Delta F_s > 0$ according to (18) (note that $\mu < 0$ in the southern hemisphere).

The zonally and JJA temporally averaged temperature difference ΔT between the control and wave drag runs is shown in Figure 6. Figure 6 is similar to Figure 1c (middle), although the meridional asymmetry in the quadrupole of the former is stronger. Possible reasons for the difference include the use of a sophisticated radiative cooling parameterization in CMAM (for which radiative relaxation times vary with latitude and altitude) as well as the existence of secondary feedbacks in CMAM, such as differences in the amount of parameterized orographic GWD between the control and wave drag runs. The latter effect turns out to play a significant role in the perturbed heating experiment considered later in this section.

The quadrupole pattern of Figure 6 is similar to those seen in some previous GCM studies. For example, *McFarlane* [1987, Figure 13] studied the effects of an orographic GWD parameterization on the Canadian Climate Centre first-generation GCM and found that the addition of a localized lower stratospheric drag resulted in a quadrupole temperature anomaly compared with a run without this drag. The shape of the quadrupole pattern suggests that this was a sponge feedback and not a transient response; the sponge in his case consisted of a Rayleigh "roof" drag applied at the uppermost model level.

In order to verify that the temperature difference seen in Figure 6 reflects the steady state behavior of CMAM, it is useful to consider (2) in the form

$$\frac{\partial T}{\partial t} + Sw = Q_s + Q_{ir}, \tag{19}$$

where Q_s and Q_{ir} represent solar heating and infrared cooling, respectively. For the special case of Newtonian cooling, $Q_{ir} = -\alpha T$ as in (2). Although not exact, (19) provides a reasonable approximation to the zonally averaged thermodynamic equation in CMAM. Subtracting the equations corresponding to (19) for the respective experiments discussed above and seasonally averaging gives

$$\frac{\Delta T_f - \Delta T_i}{\tau} + \langle S \Delta w \rangle = \langle \Delta Q_{ir} \rangle, \tag{20}$$

where ΔT_i and ΔT_f denote the difference in temperature between the control and wave drag runs at the beginning (June 1) and end (August 31) of the simulation, respectively; $\tau = 92$ days is the length of the JJA season; and the angle brackets denote the seasonal average. Since Q_s is essentially prescribed for CMAM (climatological ozone distributions are used in the model), it does not appear in (20). To establish that Figure 6 is indicative of the steady state behavior of CMAM, it is sufficient to show that the dominant balance in (20) is between the second and third terms or, equivalently, that either the second or third term in (20) is much larger than the first. (Note that it is not required that the full thermodynamic balance (19) be close to steady state.)

Figure 7a shows the first term in (20) and Figure 7b shows the third term in (20) as calculated from CMAM, both terms zonally averaged and shown in kelvins per day. Comparison of Figure 7a to 7b indicates that the term on the right-hand side of (20) is about 1 order of magnitude larger than the first term on the left-hand side. This confirms that the upper portion of the quadrupole pattern seen in Figure 6 is indeed associated with the sponge-layer feedback seen in Figure 5c.

A second experiment consists of perturbing CMAM with a source of diabatic heating (the perturbed heating run). The heating perturbation consists of a zonally symmetric Gaussian function centered on (60°S, 60 km), with a maximum amplitude of 10 K d^{-1}. The model is restarted at the beginning of May and integrated through to the end of August. The first month is discarded for the purpose of comparison with the control run described earlier.

Figure 8a shows the imposed heating perturbation, and Figure 8b shows the difference in temperature between the control run and the perturbed heating run. The region in the vicinity of the heating perturbation shows increased temperatures, as expected, while a region of reduced temperatures is seen above, extending well into the sponge layer. This aspect of the response is similar to the response seen in Figure 2c (middle). However, significant differences are also apparent.

Before discussing those differences, we first establish that the response seen in Figure 8b reflects a steady state response of CMAM. The approximate relation (20) again applies, provided the imposed heating perturbation is added to the right-hand side. Figure 9 is analogous to Figure 7, and shows that the difference in total heating (Figure 9b) has values about 1 order of magnitude larger than the difference in temperature

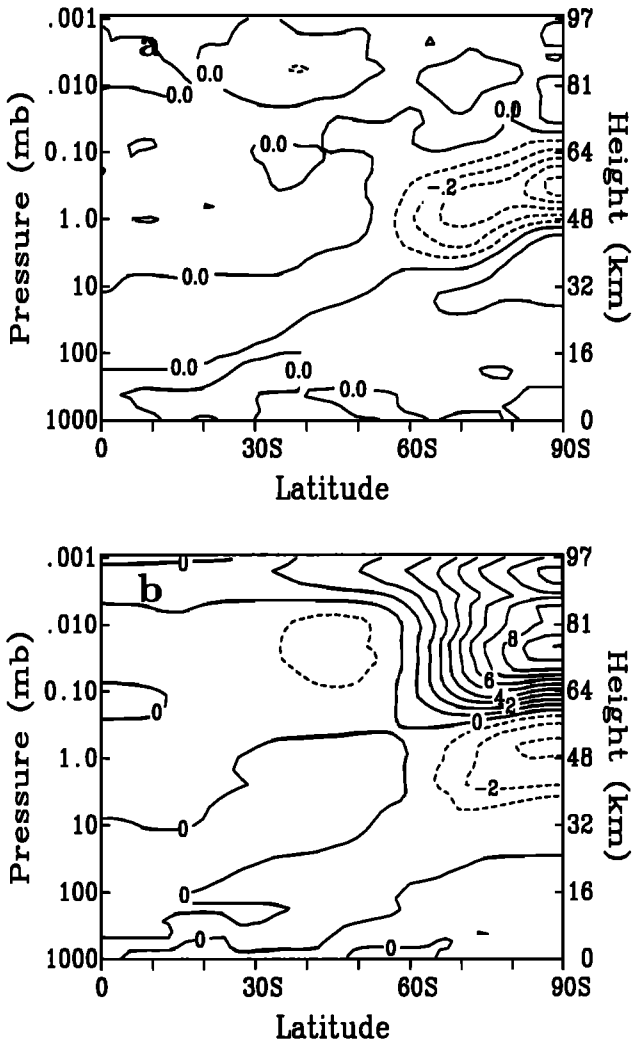

Figure 7. Zonally averaged fields appearing in (20), (a) $(\Delta T_f - \Delta T_i)/\tau$, contour interval of 0.1 K d^{-1}, and (b) $\langle \Delta Q_{ir} \rangle$, contour interval of 1 K d^{-1}. Differences between the CMAM control run and the wave drag run are denoted by Δ.

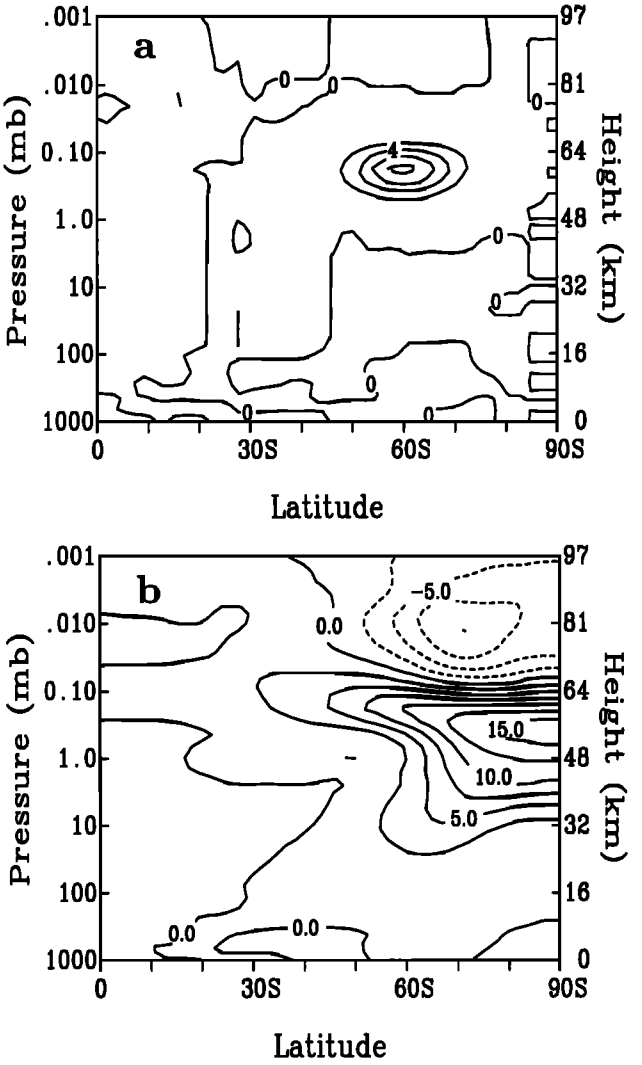

Figure 8. (a) Diabatic heating perturbation imposed in the CMAM perturbed heating run, contour interval of 2 K d^{-1}, and (b) zonally and temporally averaged temperature difference between the CMAM control run and the perturbed heating run, contour interval of 2.5 K. The temporal average is over a single June-July-August season.

tendency (Figure 9a). This confirms that the response seen in Figure 8b is a steady state response.

Yet it is clear that the sponge-layer feedback is not the only feedback in this case. In particular, the temperature increase is spread quite broadly and attains its maximum value over the pole. The difference in sponge-layer drag between the two runs, shown in Figure 10a, is positive across the sponge, instead of having the dipole structure (positive to the north and negative to the south) that one would expect from the heating perturbation alone. It turns out that these features are associated with changes in the structure of the parameterized orographic GWD, which are shown in Figure 10b. These changes induce their own response, including their own sponge-layer feedback, which together with that from the heating perturbation contribute to the temperature response seen in Figure 8b. Such "secondary feedbacks" serve to remind us that the response to an imposed extratropical local force or diabatic heating in a real middle-atmosphere model may be significantly more complex than that described in section 2. Nevertheless, sponge-layer feedbacks can be expected to be part of the response.

5. Case of a Uniform Rayleigh Drag

In sections 2–4 we have considered the case of a vertically confined upper sponge layer, which is the situation of most relevance to three-dimensional middle-atmosphere models. However, it is also of interest to consider the case of a background Rayleigh drag throughout the domain, as is commonly used in two-dimensional middle-atmosphere models [e.g., *Garcia and Solomon*, 1985; *Garcia et al.*, 1992]. Such models are

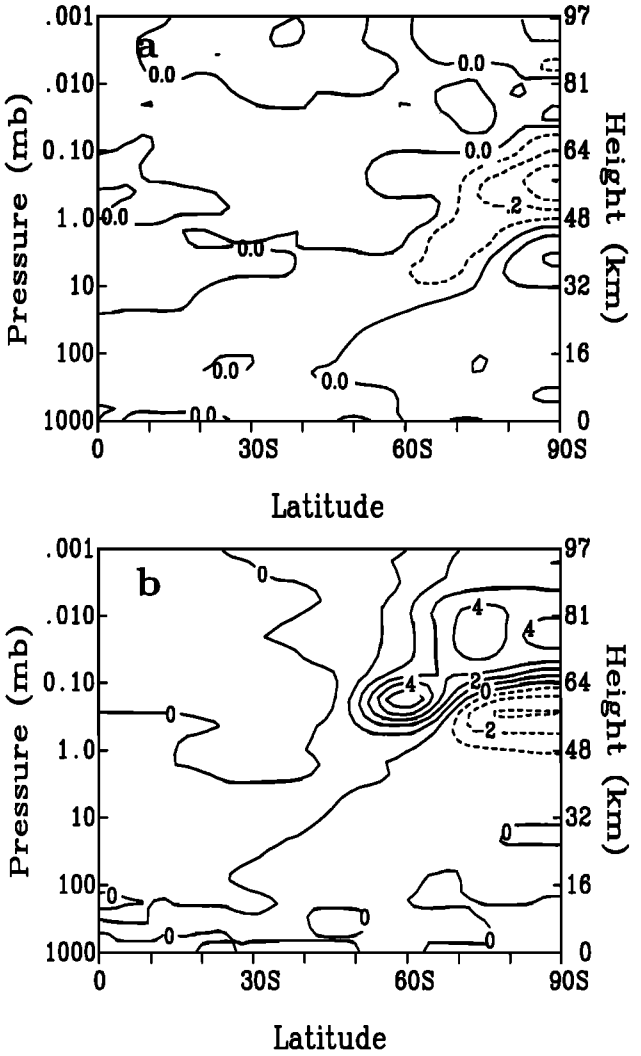

Figure 9. Zonally averaged fields, (a) $(\Delta T_f - \Delta T_i)/\tau$, contour interval of 0.1 K d^{-1}, and (b) $\langle \Delta Q \rangle$, contour interval of 1 K d^{-1}. Differences between the CMAM control run and the perturbed heating run are denoted by Δ.

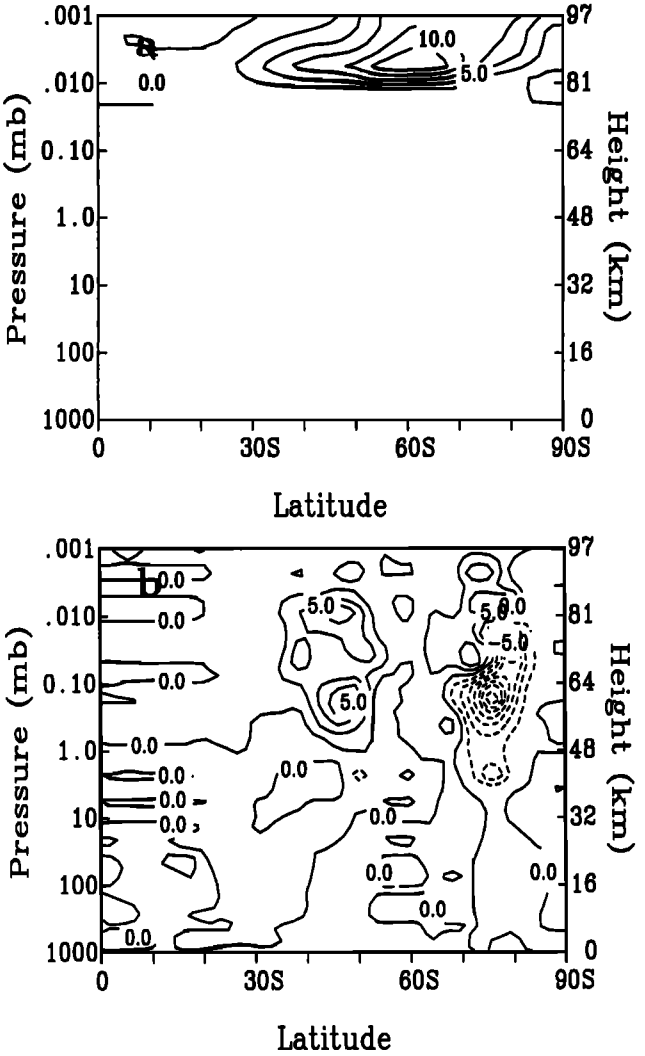

Figure 10. Zonally and temporally averaged differences in (a) sponge-layer drag and (b) orographic gravity-wave drag between the CMAM control run and the perturbed heating run. Contour interval is 2.5 m s^{-1} d^{-1}.

still widely used for climate change and impact assessment studies, because of their reduced computational cost. The impact of Rayleigh drag on the long-term response to an imposed force or diabatic heating has been previously examined by *Garcia* [1987], and *Haynes et al.* [1991] have suggested that the use of a Rayleigh drag could lead to an underestimation of downward control.

Figure 11 shows the result of an idealized numerical calculation corresponding to Figure 1c (namely, an imposed local force centered at 40 km), but with the sponge-layer drag replaced by a weak uniform background Rayleigh drag imposed throughout the model domain, with $r = 1/(100\,\text{days})$. (This is the value used by *Garcia et al.* [1992].) The instantaneous response and the long-term response in the absence of Rayleigh drag (with only the planetary boundary layer) are given as before by Figures 1a and 1b, respectively. As in section 2, we consider the downward controlled response (Figure 1b) to be the true response, and differences between Figures 1b and 11 to be a spurious Rayleigh-drag feedback. Comparing Figures 11 and 1b, it is clear that the meridional mass circulation departs from a downward controlled regime in this case (it is spread out meridionally, particularly toward lower latitudes) and that the total mass transport has been reduced by the Rayleigh drag. The temperature response is likewise distorted and is nonzero above the level of the imposed force. As for the zonal wind response, it is reduced by about a factor of 2.

Figure 12 shows the same fields as in Figure 11, but for the case of an imposed local diabatic heating as in Figure 2. Comparing Figures 12 and 2b, we again find the response to depart from a downward controlled regime in this case: there is a meridional mass circulation extending over most of the model atmosphere. The temperature response is not very different in terms of

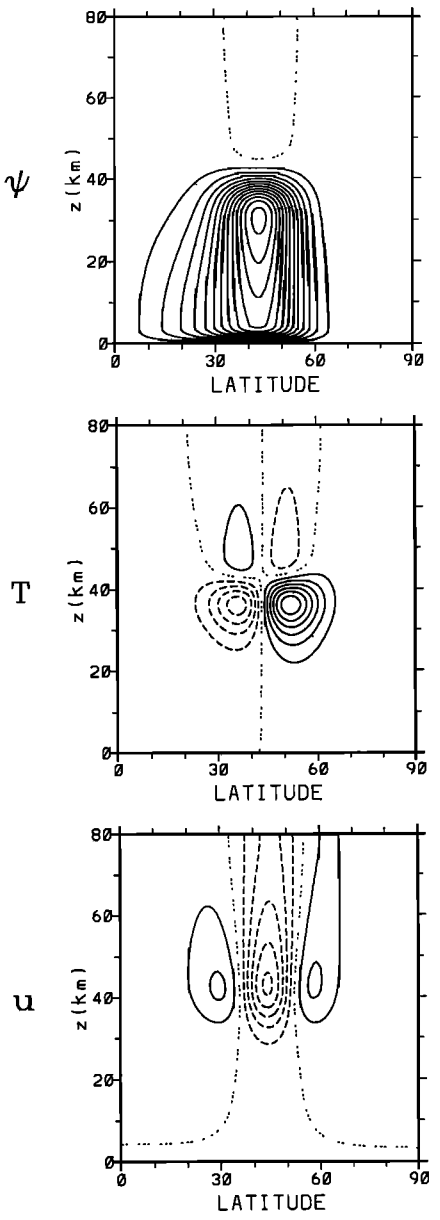

Figure 11. Same as in Figure 1c (case of imposed force), except with the sponge layer replaced by a uniform Rayleigh drag throughout the depth of the atmosphere, with $r = 1/(100\,\text{days})$. Contour intervals are as in Figure 1c.

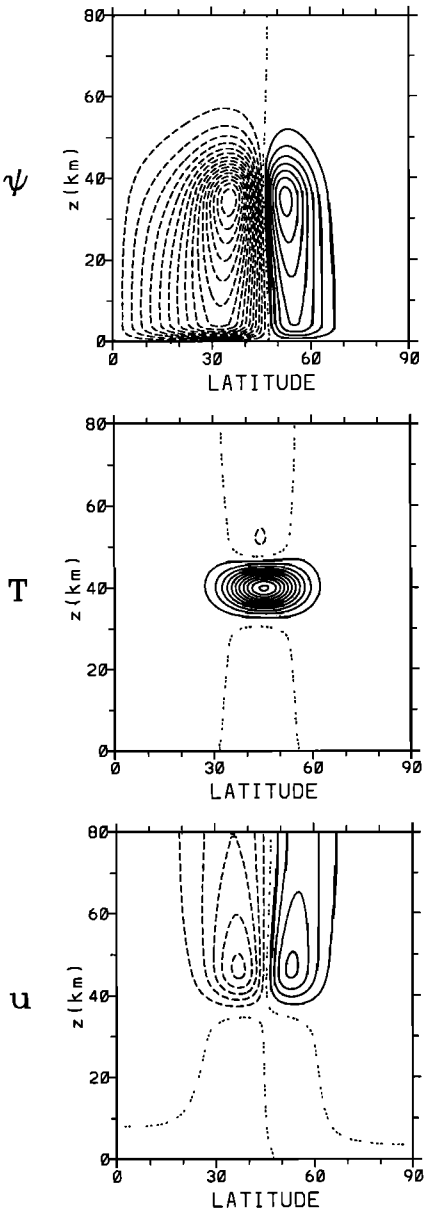

Figure 12. Same as in Figure 2c (case of imposed diabatic heating), except with the sponge layer replaced by a uniform Rayleigh drag throughout the depth of the atmosphere, with $r = 1/(100\,\text{days})$. Contour intervals are as in Figure 2c.

the maximum value of the warming, but it is spread out latitudinally so that the zonal wind response is reduced by about 20%.

We now try to understand these effects quantitatively by means of an asymptotic analysis as in section 3. We assume $r < \alpha$, which is appropriate for two-dimensional middle-atmosphere models. In this case it is convenient to ignore the boundaries altogether. We can still use the approach of *Haynes et al.* [1991], though note that it fails as $r \to \alpha$. (The propagating character of the solutions disappears when $r = \alpha$, in which case the time dependence is the same for all z, namely, $1 - e^{-\alpha t}$.)

In the case of the switch-on force $F_n(z,t) = f_n \mathcal{H}(t) \cdot \delta(z/H)$ with $Q_n = 0$, after a sufficiently long time the response is given by

$$u_n \sim \frac{f_n b_n}{2\alpha} \frac{1}{\lambda} e^{(1\mp\lambda)z/2H} \times \operatorname{erfc}\Big\{-\Big(t \mp \frac{\tilde{b}_n z}{H\alpha\lambda}\Big)\Big[\frac{H\alpha^2\lambda^3}{4\tilde{b}_n(\tilde{b}_n+\lambda^2)|z|}\Big]^{\frac{1}{2}}\Big\}, \quad (21)$$

where the minus sign in the $\mp$ is used for $z > 0$ and the plus sign for $z < 0$, $\lambda \equiv [1 + (4b_n r/\alpha)]^{\frac{1}{2}} > 1$ as before, and $\tilde{b}_n \equiv b_n(\alpha - r)/\alpha$. This has the steady state limit

$$u_n \sim \frac{f_n b_n}{\alpha} \begin{cases} \frac{1}{\lambda} e^{(1-\lambda)z/2H}, & z > 0 \\ \frac{1}{\lambda} e^{(1+\lambda)z/2H}, & z < 0 , \end{cases} \quad (22)$$

with associated temperature change

$$T_n \sim \frac{f_n N^2 H^2}{2\Omega a R \alpha} \begin{cases} \frac{1-\lambda}{2\lambda} e^{(1-\lambda)z/2H}, & z > 0 \\ \frac{1+\lambda}{2\lambda} e^{(1+\lambda)z/2H}, & z < 0 . \end{cases} \quad (23)$$

Without Rayleigh drag, $\lambda = 1$; with Rayleigh drag, $\lambda > 1$. Without Rayleigh drag, (23) implies that the temperature change in steady state is proportional to $e^{z/H}$ below the force and is zero above. With Rayleigh drag there is a more rapid decay below the force, together with a temperature change above the force of opposite sign, decaying more slowly with $|z|$ than the temperature change below [cf. *Garcia*, 1987, Figure 1]. This explains the results seen in Figures 1b (middle) and 11 (middle). As before, the latitudinal profile of the Rayleigh-drag effect will be different from that of the imposed force, because λ depends on n. (When $\lambda = 1$, in contrast, the steady state response is latitudinally localized; this is part of downward control.)

In the case of the switch-on diabatic heating $Q_n(z,t) = q_n \mathcal{H}(t)\delta(z/H)$ with $F_n = 0$, after a sufficiently long time the response is given by

$$u_n \sim \frac{q_n b_n \Omega a R}{2N^2 H^2 \alpha} \frac{(1 \pm \lambda)}{\lambda} e^{(1\mp\lambda)z/2H} \times \operatorname{erfc}\left\{ -\left(t \mp \frac{\tilde{b}_n z}{H\alpha\lambda}\right) \left[\frac{H\alpha^2\lambda^3}{4\tilde{b}_n(\tilde{b}_n + \lambda^2)|z|}\right]^{\frac{1}{2}} \right\}, \quad (24)$$

where as above the minus sign in the $\mp$ is used for $z > 0$ and the plus sign for $z < 0$, and vice-versa for the $\pm$. This has the steady state limit

$$u_n \sim \frac{q_n b_n 2\Omega a R}{N^2 H^2 \alpha} \begin{cases} \frac{1+\lambda}{2\lambda} e^{(1-\lambda)z/2H}, & z > 0 \\ \frac{1-\lambda}{2\lambda} e^{(1+\lambda)z/2H}, & z < 0 , \end{cases} \quad (25)$$

with associated temperature change

$$T_n \sim \frac{q_n}{\alpha} \begin{cases} \frac{1-\lambda^2}{4\lambda} e^{(1-\lambda)z/2H}, & z > 0 \\ \delta(z/H), & z = 0 \\ \frac{1-\lambda^2}{4\lambda} e^{(1+\lambda)z/2H}, & z < 0 . \end{cases} \quad (26)$$

Without Rayleigh drag, (26) implies that the temperature change in steady state is confined to the level of the imposed diabatic heating. With Rayleigh drag the δ function temperature change at $z = 0$ is accompanied by an oppositely signed temperature change extending above and below. The drag-induced temperature change decays more slowly with $|z|$ above than it does below. This explains the results seen in Figures 2b (middle) and 12 (middle).

6. Summary

Middle-atmosphere models commonly employ a sponge layer in the upper portion of their domain. One purpose of the sponge is to absorb vertically propagating waves, thereby preventing spurious reflections off the model lid. In this respect the sponge can be said to act realistically, with no feedback on the dynamics below. Yet the sponge is generally also allowed to act on the zonally symmetric part of the flow. In this respect it acts primarily as a surrogate for missing gravity-wave drag. The sponge-drag coefficient can, of course, be tuned so that the total sponge drag is roughly comparable to the missing gravity-wave drag, thus producing a reasonable climate. However, the sensitivity of this drag to model perturbations can be expected to be quite different in the two cases. Whereas the total gravity-wave drag is presumably determined by the strength of the tropospheric gravity-wave sources (the middle-atmosphere wind profiles only determining where the drag is deposited, not its total amount), the relaxational nature of the sponge allows it to couple to the dynamics at lower levels in an artificial manner.

This possibility, which was noted by *Haynes et al.* [1991], has been investigated by considering the problem of the long-term zonally symmetric response to an imposed extratropical quasi-steady local force or diabatic heating, extending the analysis of Haynes et al. by including an upper sponge layer in addition to the lower frictional boundary layer. In the case of an imposed force the sponge-free, downward controlled response consists of a steady meridional cell extending from the surface up to the level of the imposed force, with temperature changes confined below the forcing level. However, the sponge acts to divert a fraction of the mean meridional mass flux upward that, for realistic parameter values, is approximately equal to $\exp(-\Delta z/H)$, where Δz is the distance between the forcing region and the sponge layer and H is the density scale height. The effect on the temperature field is much more drastic; temperature changes are induced below the sponge layer that are comparable in magnitude to those found below the forcing region. In the case of an imposed diabatic heating, where the sponge-free temperature response is confined to the vicinity of the heating region, the sponge induces a meridional circulation extending through the entire depth of the atmosphere. This circulation causes temperature changes below the sponge layer that are of opposite sign and comparable in magnitude to those at the heating region.

The effects described above may be clearly seen in the idealized numerical simulations presented in Figures 1 and 2 and have been explained by an asymptotic analy-

sis of the steady state behavior (section 3). Another departure from the downward controlled response, which is particularly evident in Figure 2, is the fact that the sponge response is not as latitudinally confined as is the imposed force or diabatic heating. This feature is also accounted for by the asymptotics, since the extent of the sponge-layer feedback depends on the spatial scale of the imposed force or diabatic heating.

Having demonstrated the existence of a sponge-layer feedback, it must be emphasized that its effect on temperatures and winds decreases exponentially as one moves down from the sponge. Thus the effect of the sponge can be made arbitrarily small, at a given altitude, by placing the sponge sufficiently high; e.g., its effect on temperatures two scale heights below the sponge is roughly at the 10% level (i.e., $e^{-2} \approx 0.1$). However, this statement applies only when the imposed force or diabatic heating is located outside the sponge.

When an imposed force is located within the sponge layer (a highly plausible situation for parameterized mesospheric gravity-wave drag), the response below is severely distorted from downward control (Figure 3). In this case the force is nearly entirely absorbed within the sponge layer, and what little remains of the mass circulation is spread out over the entire hemisphere. This suggests that any parameterized force acting within a model sponge will largely fail to achieve its expected impact on temperatures below.

Some middle-atmosphere models employ a diffusive rather than a Rayleigh-drag sponge layer. Although diffusion is still relaxational, there is now a constraint that the net drag over the sphere, on a given level, must vanish. To see whether this constraint has a qualitative effect on the response, we repeated the experiment shown in Figure 1 (corresponding to an imposed force), but with the Rayleigh sponge drag $-ru$ replaced by a horizontal diffusion $\nu\nabla^2 u$, with ν ramping up between $z = 60$ km and $z = 65$ km to a value of 5×10^5 m^2 s^{-1}. (This corresponds approximately to the diffusion used by *Hack et al.* [1994].) The precise vertical dependence of ν above 60 km is the same as in (6). Figure 13 shows the response and is to be compared with Figure 1c. Evidently, the sponge-layer feedback is qualitatively the same in the two cases.

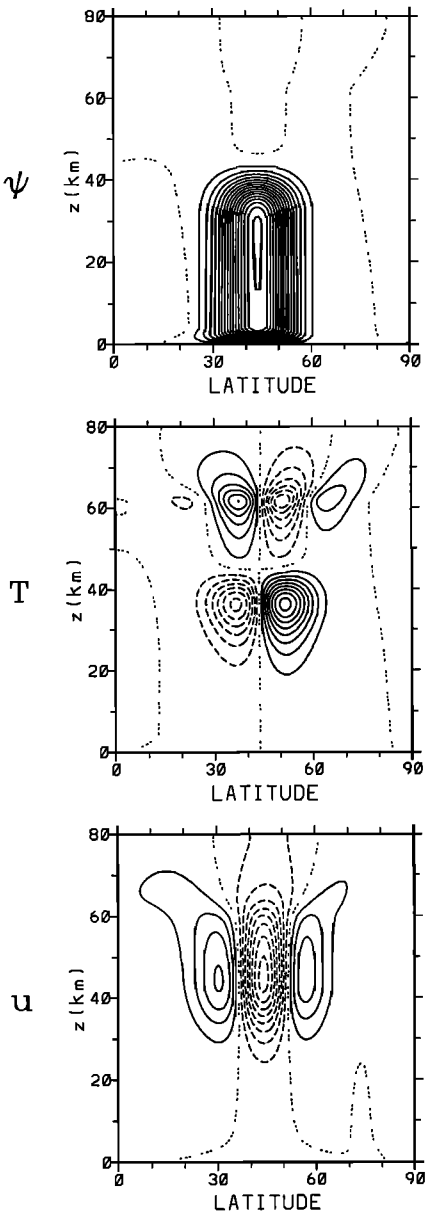

Figure 13. Same as in Figure 1c (case of imposed force), except with the Rayleigh sponge drag replaced by a strong horizontal diffusion in the sponge layer. Contour intervals are as in Figure 1c.

That the sponge-layer feedbacks in middle-atmosphere models can be important in parameter regimes of practical interest is demonstrated in section 4, where some experiments with a middle-atmosphere general circulation model are described.

The existence of this sponge-layer feedback reflects the highly nonlocal character of the zonally symmetric response problem. As *Haynes et al.* [1991] have shown, any localized force (or diabatic heating; see section 3) will induce an atmospheric response that propagates up to the top of the model. The zonal wind change in the upper part of the model will then induce a change in the sponge drag that drives a downward controlled circulation through the depth of the atmosphere, with associated effects on the temperature. That the spurious temperature changes will be comparable in magnitude, just below the sponge, to the supposedly real changes at the level of the imposed force or diabatic heating can be argued from a simple scaling analysis under the highly plausible assumption [see *Haynes et al.*, 1991, section 7] that in the transient stage, w is roughly independent of height above the level of the imposed force or diabatic heating.

The principal focus of this paper is on sponge-layer feedbacks, these being relevant to many three-dimensional models. In contrast, two-dimensional middle-atmosphere models commonly employ a background Rayleigh drag through their entire model domain (sometimes

augmented with a region of increased drag at the top). Although this drag is generally much weaker than a sponge drag, it also occurs right in the regions of interest. The possibility of a spurious Rayleigh-drag feedback in such models (a possibility also noted by *Haynes et al.* [1991]) is therefore worth considering. This problem has been studied in section 5, where it is shown that even a weak Rayleigh drag ($r = 1/(100\,\text{days})$, compared with a Newtonian cooling coefficient of $\alpha = 1/(5\,\text{days})$) leads to a distortion of the response to an imposed extratropical local force or diabatic heating. The effects are clearly seen in Figures 11 and 12 (which are to be compared with Figures 1b and 2b, respectively), and are consistent with the earlier results of *Garcia* [1987].

It should be emphasized that the results of this paper apply only to the extratropical middle atmosphere. In the tropics the downward control arguments fail to apply [*Haynes et al.*, 1991; *Holton et al.*, 1995], and the mean circulation is dominated by nonlinear, angular-momentum-conserving meridional overturning in response to time-dependent radiative driving [*Dunkerton*, 1989]. The way in which this tropical regime connects to the downward controlled extratropical regime remains to be fully elucidated and is an important area of current research.

7. Conclusions

Strong feedbacks from physical parameterizations are problematical for climate models in two distinct ways. First, when one is developing a climate model, it is important to eliminate model errors. Second, once one has a climate model that is regarded as acceptable, an important use of the model is to examine the climate change induced by natural or anthropogenic effects. Both activities involve examining the model's response to perturbations that are under the modeler's control. Clearly, it is essential that this response be physically realistic. Since physical parameterizations are usually the least reliable aspect of a climate model, strong feedbacks from those parameterizations can make the perturbed response highly unreliable.

In the extratropical middle atmosphere the kinds of perturbations discussed above can nearly always be understood in terms of changes to the wave-induced forcing F or the diabatic heating Q. We have shown that the long-term zonally symmetric response to such changes includes a strong feedback from model drag processes of a relaxational character. The particular examples that we have considered consist of an upper sponge layer (characteristic of many three-dimensional models) and a spatially uniform Rayleigh drag (characteristic of many two-dimensional models). In the case of the sponge layer the spurious component of the response has clearly identifiable features (unless the imposed force or diabatic heating is applied within the sponge layer itself, in which case the response is completely distorted). In the case of a uniform Rayleigh drag the response is noticeably distorted throughout the region of interest.

Our results have implications for the placement of model lids in three-dimensional middle-atmosphere general circulation models. Although direct observational evidence is lacking, it is widely believed that mesospheric gravity-wave drag is crucial for determining the temperature structure in the mesosphere [e.g., *Andrews et al.*, 1987], possibly down to the middle stratosphere in polar regions [*Haynes et al.*, 1991; *Garcia and Boville*, 1994]. Many middle-atmosphere modeling groups are implementing comprehensive GWD parameterization schemes, in order to try to cure the "cold pole" problems that bedevil their models. If a significant fraction (in a mass-weighted sense) of this GWD is deposited in the upper mesosphere and mesopause regions, then the arguments of this paper would suggest that any sponge layer must be applied above, say, 100 km altitude (assuming that a 10% error in the downwelling would be regarded as acceptable); since a sponge layer should itself probably be at least two scale heights deep, this would imply a model lid above 110 km. This is much higher than what is currently used in most middle-atmosphere general circulation models. Of course, it may well be that the significant GWD occurs lower down; it may also be that models can get away with damping only the non–zonal-mean part of the flow in their sponge layer. These questions remain open at the present time.

Appendix

The Hough-mode decomposition of the fields [*Plumb*, 1982] takes the form

$$v = \sum_n v_n(z,t) B_n(\mu), \qquad w = \sum_n w_n(z,t) \Theta_n(\mu),$$

$$\psi = \sum_n \psi_n(z,t)\,(1-\mu^2)^{1/2} B_n(\mu),$$

$$u = \sum_n u_n(z,t) \mu B_n(\mu), \qquad T = \sum_n T_n(z,t) \Theta_n(\mu),$$

$$F = \sum_n F_n(z,t) \mu B_n(\mu), \qquad Q = \sum_n Q_n(z,t) \Theta_n(\mu),$$

where the functions $\Theta_n(\mu)$ and $B_n(\mu)$ satisfy

$$\frac{d}{d\mu}\left\{\frac{1-\mu^2}{\mu^2}\frac{d}{d\mu}[\Theta_n(\mu)]\right\} = \epsilon_n \Theta_n(\mu),$$

$$\frac{d}{d\mu}[(1-\mu^2)^{1/2} B_n(\mu)] = \Theta_n(\mu),$$

and ϵ_n are the Hough-mode eigenvalues (listed in *Haynes et al.* [1991, Table 1]). Note that $\epsilon_n < 0$ and $|\epsilon_n| \gg 1$.

With this decomposition, (1)–(5) take the spectral form

$$\frac{\partial u_n}{\partial t} - 2\Omega v_n = F_n - r(z)u_n, \tag{A1}$$

$$\frac{\partial T_n}{\partial t} + Sw_n = Q_n - \alpha T_n, \tag{A2}$$

$$\frac{\partial u_n}{\partial z} = -\frac{\epsilon_n R T_n}{2\Omega a H}, \tag{A3}$$

$$v_n + \frac{a}{\rho_0}\frac{\partial}{\partial z}(\rho_0 w_n) = 0, \tag{A4}$$

$$v_n = -\frac{1}{\rho_0}\frac{\partial \psi_n}{\partial z}, \qquad w_n = \frac{\psi_n}{\rho_0 a}. \tag{A5}$$

Acknowledgments. This research has been supported by the Canadian MAM project, through grants from the Natural Sciences and Engineering Research Council and the Atmospheric Environment Service of Canada. K.S. acknowledges receipt of an Ontario graduate scholarship. The authors would like to thank the referees for helpful and constructive comments.

References

Andrews, D.G., J.R. Holton, and C.B. Leovy, *Middle Atmosphere Dynamics*, 489 pp., Academic, San Diego, Calif., 1987.

Boville, B.A., Middle atmosphere version of CCM2 (MA-CCM2): Annual cycle and interannual variability, *J.Geophys.Res.*, *100*, 9017–9039, 1995.

Dunkerton, T.J., Nonlinear Hadley circulation driven by asymmetric differential heating, *J.Atmos.Sci.*, *46*, 956–974, 1989.

Eliassen, A., Slow thermally or frictionally controlled meridional circulation in a circular vortex, *Astrophys.Norv.*, *5*(2), 19–60, 1951.

Garcia, R.R., On the mean meridional circulation of the middle atmosphere, *J.Atmos.Sci.*, *44*, 3599–3609, 1987.

Garcia, R.R., and B.A. Boville, "Downward control" of the mean meridional circulation and temperature distribution of the polar winter stratosphere, *J.Atmos.Sci.*, *51*, 2238–2245, 1994.

Garcia, R.R., and S. Solomon, The effect of breaking gravity waves on the dynamics and chemical composition of the mesosphere and lower thermosphere, *J.Geophys.Res.*, *90*, 3850–3868, 1985.

Garcia, R.R., F. Stordal, S. Solomon, and J.T. Kiehl, A new numerical model of the middle atmosphere, 1, Dynamics and transport of tropospheric source gases, *J.Geophys. Res.*, *97*, 12,967-12,991, 1992.

Hack, J.J., B.A. Boville, J.T. Kiehl, P.J. Rasch, and D.L. Williamson, Climate statistics from the National Center for Atmospheric Research Community Climate Model CCM2, *J.Geophys.Res.*, *99*, 20,785–20,813, 1994.

Hamilton, K., R.J. Wilson, J.D. Mahlman, and L.J. Umscheid, Climatology of the SKYHI troposphere-stratosphere-mesosphere general circulation model, *J.Atmos.Sci.*, *52*, 5–43, 1995.

Haynes, P.H., and T.G. Shepherd, The importance of surface pressure changes in the response of the atmosphere to zonally-symmetric thermal and mechanical forcing. *Quart. J.Roy.Meteor.Soc.*, *115*, 1181–1208, 1989.

Haynes, P.H., C.J. Marks, M.E. McIntyre, T.G. Shepherd, and K.P. Shine, On the "downward control" of extratropical diabatic circulations by eddy-induced mean zonal forces, *J.Atmos.Sci.*, *48*, 651–678, 1991.

Holton, J.R., The role of gravity wave induced drag and diffusion in the momentum budget of the mesosphere, *J.Atmos.Sci.*, *39*, 791–799, 1982.

Holton, J.R., P.H. Haynes, M.E. McIntyre, A.R. Douglass, R.B. Rood, and L. Pfister, Stratosphere-troposphere exchange, *Rev.Geophys.*, *33*, 403–439, 1995.

McFarlane, N.A., The effect of orographically excited gravity wave drag on the general circulation of the lower stratosphere and troposphere, *J.Atmos.Sci.*, *44*, 1775–1800, 1987.

McFarlane, N.A., G.J. Boer, J.-P. Blanchet, and M. Lazare, The Canadian Climate Centre second-generation atmospheric general circulation model and its equilibrium climate, *J.Clim.*, *5*, 1013–1044, 1992.

McIntyre, M.E., Atmospheric dynamics: Some fundamentals, with observational implications, in *The Use of EOS for Studies of Atmospheric Physics*, edited by J.C. Gille and G. Visconti, pp. 313–486, North-Holland, New York, 1992.

Plumb, R.A., Zonally symmetric Hough modes and meridional circulations in the stratosphere and mesosphere, *J.Atmos.Sci.*, *39*, 983–991, 1982.

Shepherd, T.G., The Canadian MAM project, *CMOS Bulletin*, *23*, pp. 3–12, Canadian Meteorological and Oceanographic Society, Ottawa, 1995.

Shine, K.P., Sources and sinks of zonal momentum in the middle atmosphere diagnosed using the diabatic circulation, *Quart.J.Roy.Meteor.Soc.*, *115*, 265–292, 1989.

T. G. Shepherd, K. Semeniuk, and J. N. Koshyk, Department of Physics, University of Toronto, 60 St. George Street, Toronto, Ontario, Canada M5S 1A7. (e-mail: tgs@atmosp.physics.utoronto.ca)

(Received February 28, 1996; revised June 18, 1996; accepted June 18, 1996.)